Acta Pharmaceutica Sinica B 2026;16(7):4524−4538

Chinese Pharmaceutical Association
Institute of Materia Medica, Chinese Academy of Medical Sciences

Acta Pharmaceutica Sinica B

www.elsevier.com/locate/apsb
www.sciencedirect.com

ORIGINAL ARTICLE

High-throughput ligand discovery in living cells using the cellular protein stability enhancement assay

Yue Wei[a,†], Yunyun Gao[a,†], Ruijie Li[a], Yao Chen[a], Wenjing Bai[b], Peirui Zhao[a], Junchi Hu[a], Linfeng Li[a], Xing Wang[c], Guobing Yin[c], Yongjun Dang[a,*], Xiangqian Kong[b,*], Zufeng Guo[a,*]

[a]*Basic Medicine Research and Innovation Center for Novel Target and Therapeutic Intervention (Ministry of Education), Department of Breast and Thyroid Surgery of the Second Affiliated Hospital, College of Pharmacy, Chongqing Medical University, Chongqing 400016, China*
[b]*Institute of Drug Discovery, China-New Zealand Joint Laboratory on Biomedicine and Health, Guangdong Provincial Key Laboratory of Stem Cell and Regenerative Medicine, Guangzhou Institutes of Biomedicine and Health, Chinese Academy of Sciences, Guangzhou 510530, China*
[c]*Department of Breast and Thyroid Surgery of the Second Affiliated Hospital, Chongqing Medical University, Chongqing 400016, China*

Received 17 August 2025; received in revised form 1 January 2026; accepted 3 January 2026

KEY WORDS

Target-based drug screening;
Destabilizing mutations;
KRAS;
Protein stability-based screening;
Cellular ligand discovery

Abstract Target-based drug screening typically relies on biochemical or affinity-based assays to identify compounds that modulate or bind to purified target proteins *in vitro*. However, additional cellular validation is essential to confirm genuine drug-target engagements. Integrating screening and validation within a single cellular assay could greatly expedite the drug discovery process. Herein, we developed a cellular ligand discovery method called CPSEA (cellular protein stability enhancement assay), which leverages the biophysical principle of ligand-induced stabilization of target proteins containing destabilizing mutations. Using CPSEA, we identified arteannuin B and colchicine as novel ligands for FKBP12 and $KRAS_{G12S}$, respectively. Importantly, we introduced both experimental and computational strategies to identify destabilizing mutations, thereby broadening the applicability of CPSEA for target proteins with and without known stabilizing ligands. Overall, CPSEA represents a powerful cell-based screening strategy with significant potential in target-based drug discovery.

*Corresponding authors.
E-mail addresses: yjdang@cqmu.edu.cn (Yongjun Dang), kong_xiangqian@gibh.ac.cn (Xiangqian Kong), zfguo@cqmu.edu.cn (Zufeng Guo).
[†]These authors made equal contributions to this work.
Peer review under the responsibility of Chinese Pharmaceutical Association and Institute of Materia Medica, Chinese Academy of Medical Sciences.

https://doi.org/10.1016/j.apsb.2026.02.008

1. Introduction

Most drugs achieve therapeutic effects by directly binding to target proteins, modulating their activity at functional or allosteric sites[1,2]. Extensive investigation into disease mechanisms has uncovered a multitude of potential drug targets[3], establishing target-based drug discovery (TDD) as a predominant approach in pharmaceutical research. Nevertheless, TDD has been inefficient, with only 17.3% of approved small molecule drugs since 1995 being derived from TDD[4]. This underscores the need for more effective drug discovery strategies.

Drug lead identification through TDD generally relies on *in vitro* biochemical or affinity-based screening with purified proteins, followed by cellular assays to validate drug-target engagement. However, the efficiency of these approaches for intracellular targets is relatively low, as many compounds with promising activities from the *in vitro* assays exhibit off-target effects, poor membrane permeability, or other limitations[5], thereby failing to demonstrate on-target effects *in cellulo*. Developing a cellular assay enabling simultaneous ligand screening and validation of ligand−target engagement could mitigate these issues and potentially accelerate the drug discovery process. Extensive efforts have been made to develop cellular assays that evaluate ligand−target engagement, including CETSA[6,7], DARTS[8,9], SPROX[10], LiP-SRM[11], and HIPStA[12]. Currently, only CETSA has been adapted for combination with high-throughput techniques (HT-CETSA) such as AlphaLISA[13,14] and protein-based reporters[15], enabling rapid target detection and ligand screening. With the increasing demand for high-throughput ligand screening (HTS), particularly in live-cell settings, there is growing interest in developing complementary strategies that allow highly sensitive, real-time monitoring of ligand−target engagement under physiological conditions.

A destabilizing domain (DD) is an engineered unstable protein or protein domain that incorporates one or more mutations that confer instability and promote proteasomal degradation[16]. When these destabilizing mutations are incorporated into a protein of interest (POI), the resulting DD-POI protein is rapidly degraded under untreated conditions but can be readily stabilized in the presence of a high-affinity ligand. Although this concept has been adopted to enable rapid, reversible, and dose-dependent conditional perturbation of POIs by small molecule ligands within cells[16-18], it remains uncertain whether it can be developed into a novel cellular HTS assay for ligand discovery.

In this study, we developed a cellular, destabilizing mutation-driven small molecule screening method, termed CPSEA (cellular protein stability enhancement assay). Using CPSEA, we discovered two natural products, arteannuin B and colchicine, as novel ligands for FKBP12 and $KRAS_{G12S}$, respectively. Moreover, we demonstrated the effectiveness of both deep sequencing-based approach and Gibbs free energy ($\Delta\Delta G$) prediction method in identifying unstable mutations for proteins, regardless of whether suitable ligands are available. These findings facilitate the rapid adaptation of CPSEA for ligand screening across a broader range of target proteins.

2. Materials and methods

2.1. Materials

Primary antibodies used were anti-FLAG (5174T, CST, used at a dilution of 1:1000), anti-FKBP12 (A5879, Sellect, 1:1000), anti-CypA (A5895, Sellect, 1:1000), anti-KRAS (12063-1-AP, Proteintech, 1:1000), anti-GFP (SC-9996, Santa Cruz, 1:1000), anti-β-actin (SC-47778, Santa Cruz,1:5000), anti-HSP90 (SC-69703, Santa Cruz, 1:10,000), anti-Ubiquitin (3936, CST). HRP-conjugated goat anti-mouse/-rabbit secondary antibodies were obtained from Santa Cruz (SC-516132/SC-2357, 1:10,000).

Chemicals used were MG132 (HY-13259, MCE), bafilomycin A1 (HY-100558, MCE), MLN7243 (HY-70062, MCE), FK506 (T2144, TargetMol), rapamycin (HY-10219, MCE), SLF (HY-114872, MCE), arteannuin B (T3S1447, TargetMol), CSA (T0945, TargetMol), sotorasib (T8684, TargetMol), adagrasib (T8369, TargetMol), MRTX1133 (HY-134813, MCE), BI2865 (T72062, TargetMol), erianin (T3864, TargetMol), colchicine (T0320, TargetMol), picropodophyllotoxin (T3S0027, TargetMol), combretastatin A4 (T6212, TargetMol), fosbretabulin disodium (T6272, TargetMol), colcemid (T19720, TargetMol), colchicoside (T36115, TargetMol), (*S*,*R*,*S*)-AHPC-propargyl (V287928, Aladdin).

NIH3T3 (National Collection of Authenticated Cell Cultures, SCSP-515, RRID: CVCL_0594), HEK293T (National Collection of Authenticated Cell Cultures, SCSP-5425, RRID: CVCL_0063), AGS (National Collection of Authenticated Cell Cultures, SCSP-5652, RRID: CVCL_0139), and A549 (Procell, CL-0016, RRID: CVCL_0023) were cultured in DMEM (C11995500BT, Gibco) containing 10% fetal bovine serum (10,091-148, Gibco) and 1% penicillin−streptomycin (15,140,122, Thermo Fisher Scientific). H358 (National Collection of Authenticated Cell Cultures, SCSP-583, RRID: CVCL_1559) and H520 (Procell, CL-0402, RRID: CVCL_1566) were cultured in RPMI1640 medium containing 10% fetal bovine serum and 1% penicillin−streptomycin. All cell lines were grown at 37 °C in a 5% CO_2 humidified incubator. All cell lines used in this study were regularly tested and confirmed to be free of contamination, including mycoplasma.

2.2. Plasmids

Using HEK293T cDNA as a template, the coding sequence of FKBP12 was amplified using PrimeSTAR Max DNA Polymerase (R045, TAKARA) and fused with a FLAG sequence at the N-terminus. Subsequently, EYFP was fused to the C-terminus of FKBP12 *via* fusion PCR. The FLAG-FKBP12-EYFP construct was then inserted into the lentiviral vector pCDH-CMV-MCS-EF1-Puro using Gibson assembly (C112, Vazyme). Similarly, a lentiviral vector expressing FLAG-CypA-EYFP was generated using the same approach. Additionally, point mutations (V24A, F36V) were introduced into FKBP12, and point mutations (I10F, G14C) were introduced into CypA using site-directed mutagenesis kits (C214, Vazyme).

FKBP12 and $KRAS_{WT}$ DNA sequences were amplified with HEK293T cDNA, and $KRAS_{G12C}$ and $KRAS_{G12S}$ were generated by site-directed mutation. These sequences were cloned into a pET-28a vector using Gibson assembly. The resulting constructs contain an N-terminal 6 × His tag.

2.3. Protein expression and purification

Chemically competent BL21(DE3) cells were transformed with the corresponding plasmid and cultured on LB agar plates containing 50 μg/mL kanamycin. A single colony was selected to inoculate a culture in LB supplemented with 50 μg/mL kanamycin, incubated at 37 °C and 220 rpm. When the culture reached an optical density of 0.6, the temperature was lowered to 16 °C, and protein expression was induced by adding IPTG to a final concentration of 0.5 mmol/L. After 16 h at 16 °C, the cells were harvested by centrifugation at 5000×*g* for 10 min and then lysed using a high-pressure homogenizer (Shanghai Litu) in lysis buffer (20 mmol/L Tris pH 8.0, 150 mmol/L NaCl, 20 mmol/L imidazole). The lysate was clarified by centrifugation at 15,000×*g* for 45 min. The resulting supernatant was then utilized for subsequent purification steps using immobilized metal-affinity chromatography. The supernatant was applied twice to a Ni^{2+}-NTA-affinity chromatography column, and subsequent elution was performed using 5 mL volumes of 40, 80, 110, 300, and 500 mmol/L imidazole. The target protein products were purified through gel-filtration chromatography using a Superdex 200 column (Cytiva) with a buffer containing 20 mmol/L Tris pH 8.0, 150 mmol/L NaCl, and 2 mmol/L dithiothreitol. The protein purity was assessed by SDS-PAGE and Coomassie blue staining. Following purification, the Superdex 200 gel-filtration chromatography protein was concentrated to 10 mg/mL, flash-frozen in liquid nitrogen, and stored at −80 °C for future use.

2.4. Protein library generation

Diverse sequences of FKBP12/$KRAS_{G12C}$ or other proteins were generated using error-prone PCR, employing GeneMorph II Random Mutagenesis Kit (200550, Agilent). The primer design for mismatch PCR referenced the protocol of ClonExpress II One Step Cloning Kit (C112, Vazyme). Using this protocol, error-prone PCR was theoretically expected to introduce 3−5 nucleotide mutations per 1000 bp. The resulting fragments were ligated into the vector pCDH-CMV-MCS-EF1-Puro using Gibson assembly to generate a lentivirus transfer vector. Approximately 1 μg of the ligation product was purified using the AFTspin Multifunction DNA Purification Kit (RK30100, ABclonal) and electroporated into Endura ElectroCompetent Cells (60242, Lucigen). The cells were then plated on Luria-Bertani (LB) agar plates supplemented with 100 μg/mL carbenicillin and incubated overnight at 30 °C. The following morning, all resulting colonies were scraped from the plates, and plasmid DNA was extracted using HiSpeed Plasmid Midi Kit (12643, Qiagen). This process yielded a plasmid library containing approximately 1×10^5 members.

2.5. Lentivirus package

Lentivirus was packaged through transfection of HEK293T cells using Polyethylenimine (24765, Polysciences). Transfection was performed according to the manufacturer when HEK293T cell density reached 80%. Lentivirus transfer vector, packaging plasmid psPAX2, and pMD2.G were mixed in a ratio of 4:3:1 with Polyethylenimine. The lentivirus was collected 48 and 72 h after transfection and filtered through a 0.45 μm PES membrane, and aliquoted for storage at −80 °C.

2.6. Gel electrophoresis and immunoblot

When necessary, cells were treated with drugs, reaching 50% confluency, achieving a final DMSO concentration of 1%. Following the treatment period, cells were cooled on ice. Adherent cells were rinsed once with 1 mL of ice-cold PBS, scraped using a spatula, and centrifuged at 1000×*g* for 5 min to form a pellet. Suspension cells were centrifuged at 1000×*g* for 5 min, washed with 1 mL of ice-cold PBS, and pelleted again. Cell lysis was performed on ice for 10 min using RIPA buffer (P0013D, Beyotime) supplemented with protease (B14002, Bimake) and phosphatase inhibitors (P1082, Beyotime). The resulting lysates were clarified by high-speed centrifugation at 15,000×*g* for 10 min. Lysate concentrations were determined using a BCA protein assay (C05-02001, Bioss) and adjusted to 2 mg/mL with additional RIPA buffer. Prior to analysis, samples were mixed with 5 × SDS loading dye, a crucial component, and heated at 95 °C for 5 min.

SDS-PAGE was run with 10% PAGE Gel (20325ES62, Yeasen) in a running buffer (G2027, Servicebio) at 100 V for 90 min. Protein bands were transferred from the gel to 0.2 μm nitrocellulose membranes (66485, Pall) using a wet-tank transfer apparatus in 1 × Western rapid transfer buffer (P0575, Beyotime), applying a current of 250 mA for 120 min. The membranes were then blocked in 5% bovine serum albumin (BSA) in Tris-buffered saline with Tween-20 (TBST: 20 mmol/L Tris, 150 mmol/L NaCl, 0.1% Tween-20, pH 7.6) for 1 h at room temperature. Primary antibodies were applied in 5% BSA-TBST and incubated overnight at 4 °C. Afterward, membranes were washed three times with TBST for 5 min each. Secondary antibodies diluted in 5% BSA-TBST were added according to the manufacturer's recommendations and incubated for 1 h at 23 °C. Finally, the membrane was washed three times with TBST for 5 min each and then imaged using a ChemiScope fluorescence imager (Clinx).

2.7. Proteasome inhibition assay in cell lysates

NIH3T3 cell lysates were generated by sonication in proteasome extraction buffer (50 mmol/L HEPES pH 7.8, 10 mmol/L NaCl, 1.5 mmol/L $MgCl_2$, 1 mmol/L each EDTA/EGTA, 250 mmol/L sucrose, 5 mmol/L DTT) followed by centrifugation (16,000×*g*, 10 min, 4 °C). The clarified supernatant was immediately used for subsequent analysis. For activity measurements, 50 μL aliquots of lysate were combined with 200 μL reaction mixture (extraction buffer supplemented with 2 mmol/L ATP) in opaque 96-well plates. Following 60 min incubation at 37 °C with 10 μmol/L test compounds and 100 μmol/L fluorogenic peptide substrate SUC-LLVY-AMC (S23031, Yuanye), fluorescence intensity was quantified (*E*x 360 nm/*E*m 460 nm). Proteasome activity was normalized using Eq. (1):

$$\text{Relative proteasome activity} = \left(F_{\text{Sample}} - F_{\text{Blank}}\right) / \left(F_{\text{DMSO}} - F_{\text{Blank}}\right) \quad (1)$$

Sample, DMSO, and Blank represent the small-molecule treatment group, the DMSO control group, and the background group without cell lysate, respectively.

2.8. MST assay

Purified FKBP12 or KRAS protein was thawed on ice and centrifuged at 12,000 rpm for 15 min at 4 °C. The supernatant was collected and diluted to a final concentration of 100 μmol/L in NHS buffer. The diluted KRAS or FKBP12 protein was then labeled using the Protein Labeling Kit RED-NHS 2nd Generation. After labeling, the protein was further diluted to 200 nmol/L in MST buffer. Small molecules were dissolved in DMSO and subsequently diluted in MST buffer, ensuring a consistent 2% DMSO concentration across all samples. A two-fold serial dilution was prepared in PCR tubes. Equal volumes of the labeled protein and ligand solutions were mixed and incubated at room temperature for 15 min. The prepared samples were then loaded into MST capillaries, and measurements were conducted over 10 min. Data analysis and affinity determination were performed using the instrument's built-in software.

2.9. Flow cytometry

Flow cytometry was analyzed using a BD Accuri C6 Plus instrument. Cell sorting was carried out using a BD FACSAria III Cell sorter Brochure. Data analysis was performed exclusively using FlowJo software.

2.10. Multi-round flow cytometry sorting

After packaging the mutation library into lentivirus, NIH3T3 cells were infected at an MOI of 0.2. 24 h post-infection, the medium was replaced with fresh culture medium, and then 2 μg/mL puromycin was added for selection after another 24 h. Following 48 h of puromycin selection, NIH3T3 cells expressing the mutation library were obtained. Ligand small molecules for the proteins (FKBP12: 5 μmol/L FK506; $KRAS_{G12C}$: 5 μmol/L sotorasib) were added and incubated for 48 h. After treatment, cells underwent flow cytometry sorting based on EYFP fluorescence intensity to select the top 5% of cells with high fluorescence intensity. The sorted cells were expanded in culture and treated with fresh medium without ligand for 48 h. Then, the bottom 5% of cells with low fluorescence intensity were sorted again. This process of flow cytometry sorting was repeated for a total of three rounds. The expanded cells from the final round of sorting were collected.

2.11. Flow cytometry sorting combined with illumina sequencing

After obtaining NIH3T3 cells expressing the mutant protein library, cells were treated with the corresponding ligand small molecules or an equal volume of DMSO for 48 h. Flow cytometry was then performed to sort cells based on EYFP fluorescence intensity into five bins, and cells were collected accordingly. gDNA was extracted from the collected cells using Genomic DNA Kit (DP304-02, TIANGEN Biotech), protein fragments were PCR-amplified using PrimeSTAR Max DNA Polymerase (R045, TAKARA), and then subjected to Illumina sequencing. Specific PCR products were sent to Sangon Biotech (Shanghai, China) for sequencing library preparation and sequencing.

Library preparation was carried out in two steps of PCR. A reaction mixture containing DNA, amplicon PCR forward and reverse primers, and PCR Ready Mix (09420398001, Roche) was prepared and subjected to thermal cycling for the first round of PCR. The resulting PCR products were analyzed by gel electrophoresis and then underwent a thorough purification process using AMPure XP beads (A63882, Beckman coulter). This meticulous purification process ensures the highest quality of the samples. Following this, a second round of PCR was performed to add Illumina P5 and P7 adaptors and indexes with DNA, universal primers with indexes, and PCR Ready Mix. The thermal cycling conditions were set accordingly, and the resulting PCR products were purified again using AMPure XP beads. The libraries were then quantified and pooled. Paired-end sequencing of the library was performed on the NovaSeq6000 with PE300 model (Illumina, San Diego, CA, USA).

2.12. Data QC and sequence calculation

Raw reads were filtered according to three steps: 1) Removing adaptor sequence if reads contain by cutadapt (v1.2.1); 2) Removing low-quality bases from reads 3′ to 5′ ($Q < 20$) by PRINSEQ-lite (v0.20.3); 3) Removing chimera sequence by usearch software (v11.0.667) with *de novo* mode by default parameter. The remaining clean data were used for further analysis. A Python script was briefly used to pick up the target sequence when both forward and reverse primer perfectly matched, then calculate the unique and total sequences.

2.13. Calculation of mutant protein fluorescence intensity

The obtained nucleotide sequences were translated into amino acid sequences, excluding sequences with premature stop mutations, and consolidating synonymous nucleotide mutations. The data were normalized to obtain the distribution of different amino acid mutations across the various bins under drug-treated and untreated conditions. Based on the distribution of nucleotide sequences corresponding to different amino acid mutations across each bin, we calculated the fluorescence intensity of different mutations before and after ligand treatment.

The formula to calculate the PSI for untreated samples is as Eq. (2):

$$\mathrm{PSI(mutation)} = \sum_{i=1}^{5} (R_i * i) \tag{2}$$

where R_i represents the fraction of reads of the mutation in bin_i for the untreated group.

Taking the V24A mutant of FKBP12 as an example, in the ligand-free condition, the number of reads in bins_{1-5} was 1, 11, 11, 24, and 25, respectively. The corresponding R_{1-5} values were 0, 0.25, 0.38, 0.31, and 0.06, respectively. Therefore, the PSI(V24A) is calculated as Eq. (3):

$$\begin{aligned}\mathrm{PSI\ (V24A)} = {} & 0*1 + 0.25*2 + 0.38*3 + 0.31*4 \\ & + 0.06*5 = 3.18\end{aligned} \tag{3}$$

The formula to calculate the PSI for samples treated with ligand is as Eq. (4):

$$\mathrm{PSI\ (mutation\ with\ ligand)} = \sum_{i=1}^{5} (R_i * i) \tag{4}$$

where R_i represents the fraction of the mutation in bin_i for the ligand-treated group.

Taking the V24A mutant of FKBP12 as an example, in the ligand condition, the number of reads in bins_{1-5} was 1, 11, 11, 24, and 25, respectively. The corresponding R_{1-5} values were 0.01, 0.15, 0.18, 0.33, and 0.35, respectively. Therefore, the PSI (V24A

with ligand) is calculated as Eq. (5):

$$\text{PSI (V24A with ligand)} = 0.01*1 + 0.15*2 + 0.15*3 + 0.33*4 + 0.35*5 = 3.83 \quad (5)$$

The folding fitness represents the change in stability of a mutated protein after mutation, calculated using Eq. (6):

$$\text{Folding fitness (mutation)} = \text{Log}_{10}\left(\frac{\text{PSI(mutation)}}{\text{PSI(WT)}}\right) \quad (6)$$

Taking FKBP12 wild-type as an example, the number of reads in bins_{1-5} was 9659, 26,225, 44,541, 51,481, and 59,540, respectively. The corresponding R_{1-5} values were 0.05, 0.14, 0.23, 0.27, and 0.31, respectively. Therefore, the PSI (WT) is calculated as Eqs. (7) and (8):

$$\text{PSI (WT)} = 0.05*1 + 0.14*2 + 0.23*3 + 0.27*4 + 0.31*5 = 3.65 \quad (7)$$

$$\text{Folding fitness (V24A)} = \text{Log}_{10}(3.83/3.65) = -0.06 \quad (8)$$

2.14. High-throughput ligand screening

In this project, we screened two natural product compound libraries of different sizes. For method validation with the DD-FKBP12 protein, we selected a smaller library containing 960 compounds, most of which have experimentally validated pharmacological activities. For screening against the DD-$\text{KRAS}_{\text{G12C}}$, we used a larger library, L6000, comprising 2592 compounds. These compounds are derived from natural sources, including over 2000 species of medicinal plants, animals, and microorganisms, covering more than 500 distinct scaffold structures and over 1000 target receptors. High-throughput ligand screening was conducted using NIH3T3 cells expressing destabilizing domains proteins seeded into a 96-well Round Bottom Plate (163,320, Thermo Scientific) at 10,000 cells per well in a final volume of 100 μL. Drug treatments were performed using high-throughput drug screening system (Explorer G3, PerkinElmer) at a final concentration of 10 μmol/L for 24 h. Following treatment, the culture medium was aspirated, and each well was washed with 100 μL of PBS to rinse the cells. Subsequently, 15 μL of trypsin (C0209, Beyotime) was added to digest the cells, and the digestion was terminated using PBS containing 10% FBS. High-throughput flow cytometry analysis was conducted using a Intellicyt iQue3 flow cytometer (Sartorius) to measure the EYFP fluorescence intensity and cell count per well. Wells with a cell viability rate (number of cells in experimental group divided by number of cells in DMSO control group) greater than 50% were considered valid data. In the DD-FKBP12 screening model, cells treated with 5 μmol/L FK506 were considered positive (100% fluorescence intensity), while in the DD-KRAS screening model, cells treated with 5 μmol/L Sotorasib were considered positive, and those treated with DMSO (0% fluorescence intensity) were considered negative. The Z' factor was calculated to assess assay quality and screening window using Eq. (9):

$$Z'\text{factor} = 1 - 3(\sigma_p + \sigma_n) / |\mu_p - \mu_n| \quad (9)$$

where σ_p and σ_n represent the standard deviations of the positive and negative controls, respectively, while μ_p and μ_n denote their mean values. Positive hits were selected based on Z-score >3. Z-scores were derived from Relative MFI (compound/DMSO) using Eq. (10):

$$Z - \text{score} = (X_i - \mu_n) / \sigma_n \quad (10)$$

where X_i represent the relative MFI of the compound-treated sample.

After identifying positive hits in the primary screen, we re-treated the corresponding cell models with compounds at different concentration gradients, following the same procedure as before. The only difference was that after detaching the cells and stopping the digestion, propidium iodide (PI) was added at a final concentration of 0.05 mg/mL and incubated at room temperature for 10 min before flow cytometry analysis. During data analysis, PI-stained dead cells were excluded, and the EYFP fluorescence intensity of the remaining cells was analyzed. Additionally, compounds that interfere with intracellular processes such as transcription, translation, or protein degradation may also enhance the fluorescence signal of DD-POI-EYFP. To exclude these false-positive hits, we performed orthogonal validation using the DD-CypA-EYFP system. Specifically, NIH3T3 cells expressing DD-CypA-EYFP were treated with the same concentration of compounds for an identical duration. Compounds that significantly increased the fluorescence signal in the DD-CypA-EYFP system were excluded, as the likelihood of a compound simultaneously binding both the POI and CypA is extremely low.

2.15. Cellular thermal shift assay

For the cellular thermal shift assay, cells were treated with either DMSO or the indicated compound at indicated concentrations in fresh media for 3 h at 37 °C. Subsequently, the cells were harvested, washed once with binding buffer (cold PBS containing DMSO or the specified compound and protease inhibitor cocktail), and resuspended in 1.5 mL of binding buffer. Next, 100 μL aliquots of the cell suspension were transferred to PCR tubes and heated at specified temperatures using a Bio-Rad C1000 Thermal Cycler for 3 min, followed by a 3 min incubation at 25 °C. After three snap freeze-thaw cycles using liquid nitrogen, the lysates were transferred to 1.5 mL Eppendorf tubes and centrifuged at 15,000×g for 20 min at 4 °C. The resulting supernatant was transferred to new Eppendorf tubes, mixed with 5 × loading buffer, boiled for 15 min, and then subjected to immunoblotting.

2.16. Thermal shift assays

Recombinant FKBP12 WT and mutant proteins were diluted to a final concentration of 100 μmol/L and mixed with 50 × SYPRO Orange dye. Each reaction contained 3 μL PBS, 6 μL of 100 μmol/L protein, and 6 μL of 50 × SYPRO Orange. All samples were analyzed in triplicate. Reactions were loaded into a 96-well white qPCR plate, followed by a temperature gradient from 25 to 85 °C at a ramp rate of 0.15 °C/s. Fluorescence intensity was recorded continuously, and melting curves were generated based on SYPRO Orange fluorescence enhancement caused by exposure of hydrophobic residues during protein unfolding. The apparent melting temperature (T_m) was obtained by fitting the denaturation curves using a Boltzmann sigmoidal model. Comparative analysis

of T_m values was used to assess differences in intrinsic protein stability.

2.17. Circular dichroism spectroscopy

Circular dichroism spectroscopy was performed to evaluate secondary structure alterations in wild-type and mutant FKBP12 proteins, as well as structural changes upon FK506 binding. Purified proteins were diluted in PBS to 0.2 mg/mL, and 20 μmol/L FK506 or an equal volume of DMSO was added. Samples were loaded into 1-mm quartz cuvettes and scanned from 190 to 260 nm at a speed of 1 nm/s using a CD spectrometer. Spectra were corrected by subtracting buffer baselines and converted to mean residue ellipticity (MRE). CD spectra of wild-type and mutant proteins in DMSO were compared to evaluate the structural impact of destabilizing mutations. Differences between DMSO- and FK506-treated samples were used to assess whether ligand binding promotes partial restoration of the native fold. Secondary structure composition was estimated using the BeStSel online analysis tool.

2.18. Co-immunoprecipitation

Co-immunoprecipitation was performed to determine whether arteannuin B or colchicine alters the ubiquitination levels of FKBP12 or KRAS. NIH3T3 cells expressing FLAG-tagged FKBP12 or $KRAS_{G12C}$ were treated with 5 μmol/L compound (arteannuin B, colchicine, erianin) or DMSO for 24 h. Cells were lysed, and a portion of the lysate was retained as input. Equal amounts of protein lysate were incubated with anti-FLAG antibody-conjugated magnetic beads at 4 °C for 2 h with rotation. Beads were washed extensively and eluted in 1 × SDS−PAGE loading buffer at 95 °C for 5 min. Ubiquitination of FKBP12 or KRAS was assessed by Western blotting using anti-ubiquitin antibodies, while immunoprecipitation efficiency was evaluated using anti-FKBP12 or anti-KRAS antibodies.

2.19. Molecular docking assay

Molecular docking was performed to predict the binding mode and affinity of the ligands to the target protein. The three-dimensional structure of the target protein was obtained from the Protein Data Bank ($KRAS_{G12S}$ PDB ID: 7TLE[19]). Prior to docking, the protein structure was prepared by removing water molecules, adding hydrogen atoms, optimizing the protonation states of the residues, and locally minimizing the energy using Protein Preparation Wizard in Maestro. The ligands were rationally ionized and energetically minimized using LigPrep module. All prepared proteins and ligands were converted to PDBQT files using AutoDock Tools. For KRAS mutants, side chains of residues around the ligands were set to be flexible and corresponding receptors files were also generated. Based on the existing ligand, a grid box with an appropriate size and center was set to encompass the binding pocket. Docking simulations were carried out using AutoDock Vina, with a specified exhaustiveness of 16. The top-scored poses were manually analyzed to determine the binding modes of the ligands. The interactions between the ligands and the target protein were visualized using PyMOL.

3. Results

3.1. Design of a ligand screening platform using destabilizing domains

To evaluate whether the dd-based approach can be used to develop a ligand screening platform, we first investigated the well-characterized immunophilin FKBP12. As previously reported, FKBP12 harboring mutations such as V24A and F36V (designated as DD-FKBP12, Supporting Information Fig. S1a) is inherently unstable, leading to rapid degradation of its fusion protein with enhanced yellow fluorescent protein (EYFP) *via* the proteasome system. In DD-FKBP12, the V24A mutation destabilizes FKBP12 itself[16], while F36V creates a cavity that increases its affinity for certain ligands[20]. As expected, treatment with the small molecule ligand SLF effectively stabilized DD-FKBP12-EYFP fusion protein during flow cytometry analysis (Fig. 1a and b)[21].

To determine whether other FKBP12 ligands, FK506[22] and rapamycin[23], which share similar FKBP-binding domain (FKBD) structures with SLF (Fig. S1b−d), can similarly stabilize DD-FKBP12, we generated NIH3T3 cells expressing the DD-FKBP12-EYFP fusion protein and treated these cells with the ligands. The relative mean fluorescence intensity (MFI) significantly increased upon ligand treatment, indicating that ligand binding enhanced DD-FKBP12 stability (Fig. 1b). In contrast, these compounds exerted much less effects on wild-type FKBP12-EYFP (wtFKBP12-EYFP) (Fig. 1c). Western blot analysis corroborated these findings, showing that the severely reduced steady-state level of DD-FKBP12-EYFP was restored to levels comparable to wtFKBP12-EYFP upon treatment with FKBP12 binders, especially FK506 and rapamycin (Fig. 1d). This fluorescence enhancement was also evident in HEK293T cells, confirming the strategy's applicability in human cells (Fig. S1e). Moreover, circular dichroism (CD) spectra provided additional evidence for the stabilizing effect of ligand binding on DD-FKBP12, showing partial restoration of its native conformation upon FK506 binding (Fig. S1f and g). Consistently, microscale thermophoresis (MST)-based binding assays indicated that introducing destabilizing mutations into recombinant FKBP12 did not significantly alter its ligand-binding affinity (Fig. S1h).

Similarly, NIH3T3 cells expressing DD-CypA-EYFP (Cyclophilin A harboring I10F and G14C double mutations)[24] were treated with the ligands cyclosporin A (CSA)[25] and sanglifehrin A (SFA)[26], which possess different skeletons and binding modes (Fig. S1i−k). Both ligands stabilized DD-CypA-EYFP in a concentration-dependent manner (Fig. 1e), while having only a subtle-to-minimal impact on wtCypA-EYFP (Fig. 1f and g). These findings underscore the value of the DD-protein-based approach in providing a unique window for evaluating the on-target engagements of different ligands in living cells. Given this method is based on the biophysical principle of ligand-induced stabilization of DD-proteins within cellular environments, we named it CPSEA (cellular protein stability enhancement assay).

3.2. Identification of arteannuin B as a novel ligand for FKBP12 using CPSEA

To assess the feasibility of CPSEA in discovering new ligands, we employed DD-FKBP12-EYFP as a proof-of-concept model to screen a library containing 960 natural products, the majority of

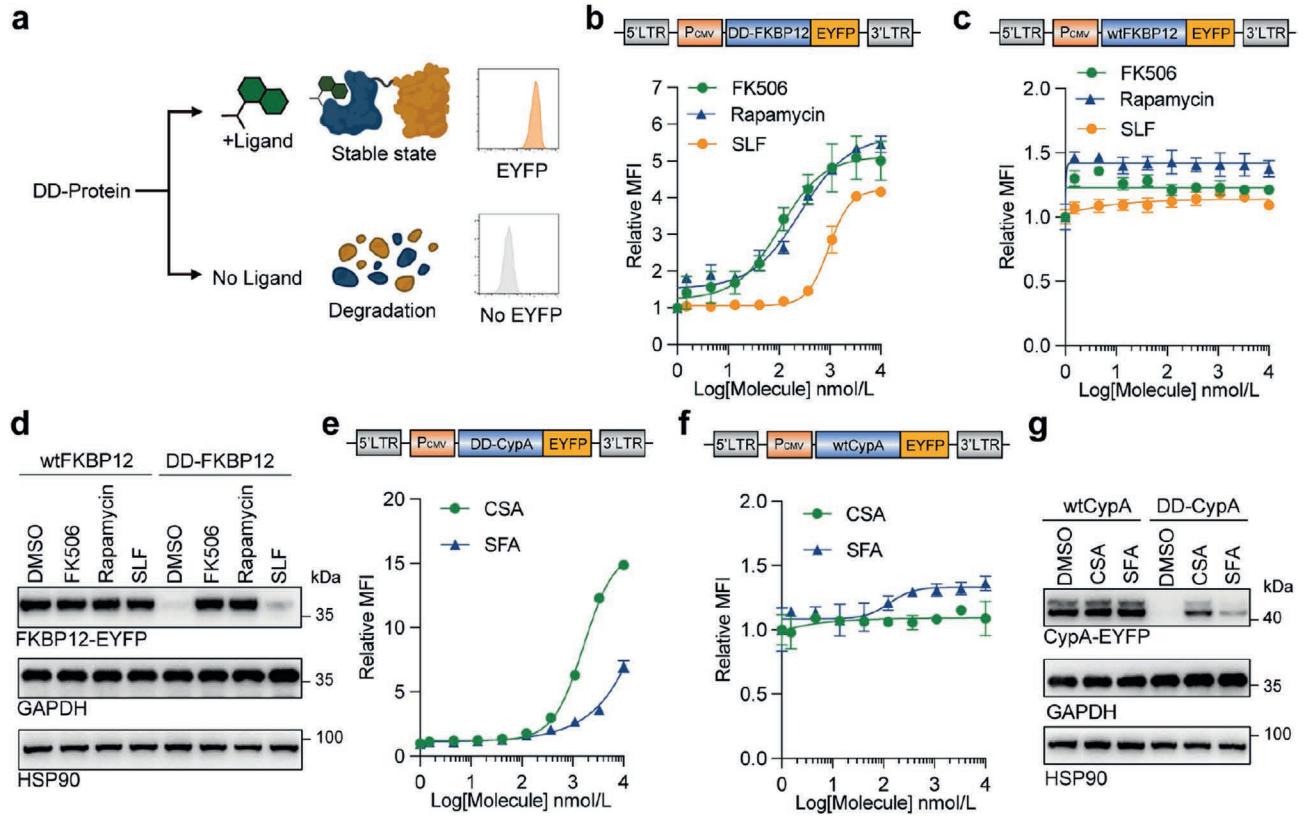

Figure 1 Design of a ligand screening platform using destabilizing domains. (a) Schematic representation of DD-protein's response to ligand. (b) Dose-dependent stabilization of DD-FKBP12-EYFP by various ligands. NIH3T3 cells expressing DD-FKBP12-EYFP were treated with 1.52−10,000 nmol/L specified ligand for 24 h, and MFI of EYFP was analyzed using flow cytometry. Relative MFI represents the MFI of ligand-treated cells relative to the MFI of DMSO-treated cells. (c) Ligand addition induces only a minor change in relative MFI in cells expressing wtFKBP12-EYFP. (d) NIH3T3 cells expressing DD/wtFKBP12-EYFP were treated with 5 μmol/L specified ligand for 24 h. FKBP12-EYFP levels were measured by Western blot. (e) NIH3T3 cells expressing DD-CypA-EYFP were treated with 1.52−10,000 nmol/L specified ligand for 24 h. (f) Ligand addition induces only a minor change in relative MFI in cells expressing wtCypA-EYFP. (g) NIH3T3 cells expressing DD/wtCypA-EYFP were treated with 5 μmol/L specified ligand for 24 h. CypA-EYFP levels were measured by Western blot. Data in (b, c, e, f) (derived from three independent experiments) represent the mean ± SD of four technical replicates from one representative experiment. A representative of three independent experiments is shown in (d, g).

which have experimentally validated pharmacological activities (Fig. 2a). Since DD-proteins are generally degraded through the ubiquitin-proteasome system[21], we hypothesized that proteasome inhibitors could prevent this degradation and thereby enhance the fluorescence signal. Consequently, the proteasome inhibitor MG132 was included as a positive control alongside FK506. Our HTS model achieved an averaged Z' factor of 0.76 (Supporting Information Fig. S2a), indicating a robust assay. Using a Z-score >3 as the threshold for hit-selection during the primary screening, and incorporating a propidium iodide (PI) staining step to exclude fluorescence from dead cells in the counter-screen, we identified a total of five hits (Fig. 2b).

Among these, arteannuin B dose-dependently increased DD-FKBP12-EYFP signals (EC_{50} = 2.14 μmol/L; Fig. 2c, Fig. S2b and c) without affecting FKBP12 transcription (Fig. S2d), DD-CypA-EYFP reporter activity (Fig. 2d), global or FKBP12 ubiquitination (Fig. S2e and f), and proteasome activity (Fig. S2g). These observations suggest that the fluorescence increase is indicative of arteannuin B's direct binding to FKBP12. Supporting this, MST studies revealed potent binding of arteannuin B to purified, wild-type FKBP12 protein (K_d = 412 ± 37 nmol/L, Fig. 2e), and CETSA assays confirmed enhanced thermal stability of endogenous FKBP12 upon treatment (Fig. 2f and Fig. S2h). As anticipated[27], arteannuin B activated the bone morphogenetic protein (BMP) reporter gene in an FKBP12-depedent manner (Fig. S2i). Collectively, these results demonstrate the potential of CPSEA in identifying structurally novel and cellularly active protein binders.

3.3. Development of an optimized, deep sequencing-based approach for identifying protein destabilizing mutations

While the above data established that CPESA represents an efficient ligand screening strategy, the destabilizing mutations in most proteins remain uncharacterized. Therefore, developing a broadly applicable protocol to detect destabilizing mutations will enhance the utility of CPESA. To this end, we first evaluated a strategy similar to that reported previously[16], which combines error-prone PCR and screening of a mutant protein library, on the small GTPase KRAS. The missense mutations at codon 12 (G12) of KRAS act as oncogenic drivers for human cancers[28], yet reliable

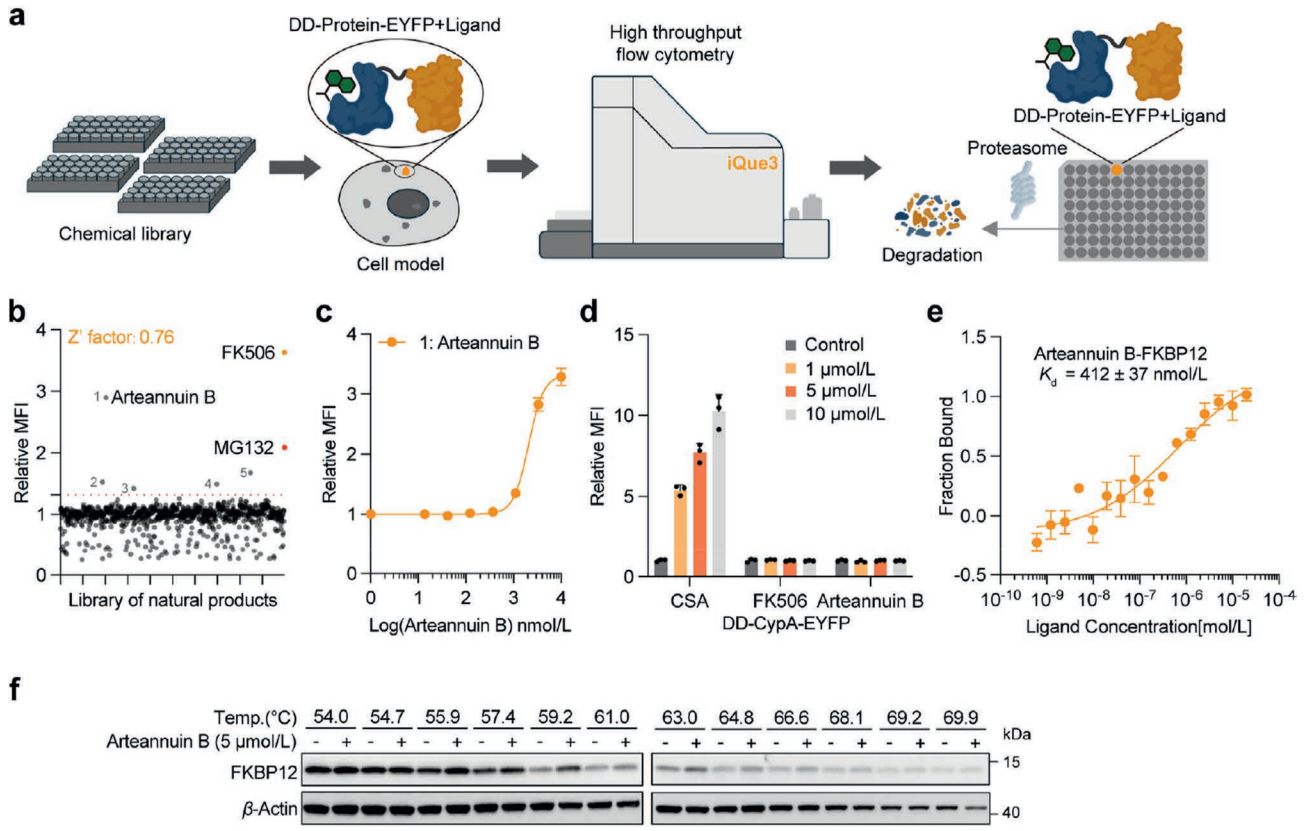

Figure 2 Identification of arteannuin B as a novel ligand for FKBP12 using CPSEA. (a) Schematic diagram of high-throughput ligand screening using CPSEA. (b) Scatter plot of primary screening data showing compounds from a library of natural products that stabilize DD-FKBP12. NIH3T3 cells expressing DD-FKBP12-EYFP were treated with 5 μmol/L compounds for 24 h and the MFI of EYFP was analyzed using flow cytometry. Relative MFI represents the MFI of compound-treated cells relative to the MFI of DMSO-treated cells. The red dashed line represents the position of the Relative MFI at a *Z*-score of 3. 1: arteannuin B; 2: lycorine; 3: oleanolic acid; 4: curcumin; 5: brevilin A. (c) Dose-dependent stabilization of DD-FKBP12-EYFP by arteannuin B. NIH3T3 cells expressing DD-FKBP12-EYFP were treated with 13.7−10,000 nmol/L arteannuin B for 24 h. Before analyzing the EYFP fluorescence signal, dead cell populations were excluded using PI dye. (d) NIH3T3 cells expressing DD-CypA-EYFP were treated with specified compounds for 24 h. (e) MST assay showing the interaction between FKBP12 and arteannuin B. (f) Thermal stability of FKBP12 in HEK 293T cells in response to arteannuin B as assessed by CETSA. Data in (c−e) (representative of two independent experiments) show means ± SD from three technical replicates per experiment.

cellular HTS methods for these mutants are lacking. A library of approximately 100,000 random gene mutations was generated through error-prone PCR for $KRAS_{G12C}$ cancer-driving mutant. As a control, a similar mutant library was created for FKBP12 (Fig. 3a). Using sotorasib and FK506 as stabilizers for $KRAS_{G12C}$ and FKBP12, respectively, we conducted three rounds of fluorescence-activated cell sorting (FACS) to enrich for cells with the highest fluorescence signals under ligand treatment and the lowest signals without ligand (Supporting Information Fig. S3a)[16]. Although we successfully obtained such mutant cell population for FKBP12, this process failed to do so for the $KRAS_{G12C}$ library (Fig. S3b and c). These results accentuated the need for a more efficient, universally applicable method.

We speculated that the destabilizing mutations may impose growth disadvantages, hindering enrichment during repeated FACS studies. Accordingly, we coupled the mutant library screening with amplicon deep sequencing analysis to avoid long-term cell culture (Fig. 3b). Briefly, cells harboring random mutations were sorted into different bins based on EYFP signal intensity, representing varying stability levels. Mutations causing protein instability tended to be enriched in bins with lower EYFP signals, while ligand binding shifted them toward bins with higher EYFP signals. Deep sequencing in each bin allowed for the identification of destabilizing mutations associated with significant EYFP changes.

The practicability of this method was first evaluated using cells expressing the FKBP12-EYFP mutants. After treatment with DMSO or FK506, cells were sorted into five bins according to EYFP signals. To quantitatively assess the stability of each mutant, we introduced a protein stability index (PSI), calculated from protein distribution across each bin as reported before[29]. Specifically, we assigned weights of 1 to 5 to the bins, and the PSI was defined using the formula (Fig. 3c) where i represents the bin number (ranging from 1 to 5), and R_i is the fraction of the total signal present in bin_i. A higher PSI indicates greater protein stability, which shifted rightward following the addition of FK506 (Fig. 3c). Based on PSI analysis, a subset of mutants with high fold changes and read counts was selected (Fig. 3d), and cells expressing these mutants were preferentially distributed in bins with higher fluorescence intensity upon FK506 treatment (Fig. S3d). Interestingly, these mutations variably affected FKBP12 stability but collectively responded robustly to ligand addition,

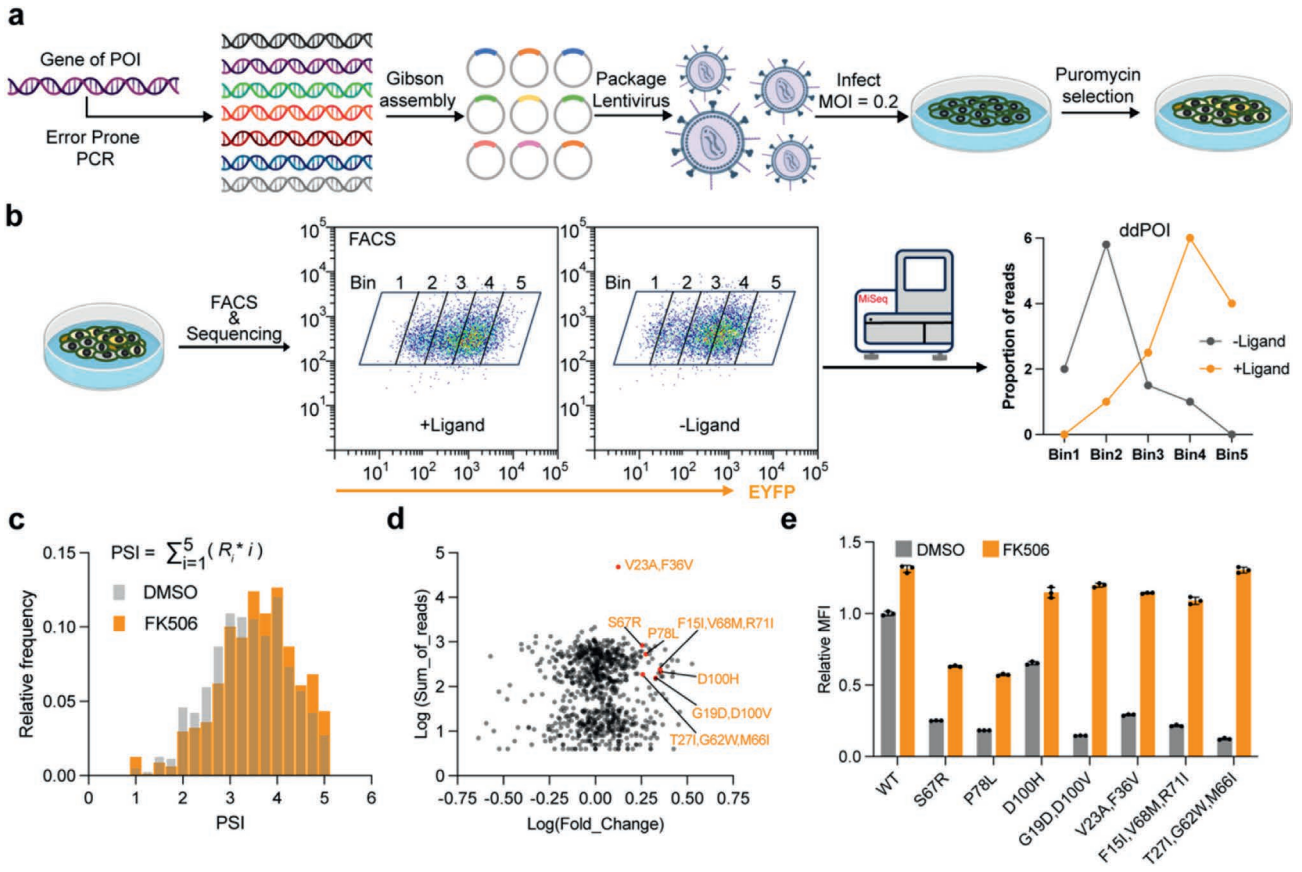

Figure 3 Development of an optimized, deep sequencing-based approach for identifying protein destabilizing mutations. (a) Schematic representation of the steps to obtain cells stably expressing the mutant library of POI. (b) Schematic representation of the steps to obtain DD-POI by FACS and sequencing. (c) Overall distribution of stability scores of mutant FKBP12, comparing DMSO-treated (grey) and FK506-treated (yellow) cells. (d) The distribution of sequencing reads and the stability changes of approximately 800 mutant FKBP12 before and after FK506 treatment. The fold change represents the ratio of PSI in mutant cells after FK506 treatment compared to untreated cells, while the sum of reads represents the total number of nucleic acid sequence reads from deep sequencing corresponding to each amino acid mutation. The red points were selected for subsequent experimental validation. (e) Histogram showing the relative MFI of various mutant FKBP12. NIH3T3 cells expressing specified mutant FKBP12 were treated with 5 μmol/L FK506 or DMSO for 24 h, and MFI of EYFP was analyzed using flow cytometry. The relative MFI represents the MFI of cells relative to the MFI of DMSO-treated NIH3T3 cells expressing wtFKBP12. The data represent the mean ± SD from three technical replicates and the experiments were repeated three times.

particularly for those double or triple mutants (Fig. 3e). These findings demonstrate that this deep sequencing-based approach could serve as an effective means to identify protein-destabilizing mutations.

3.4. Identification and characterization of DD-KRAS

Next, we applied the described approach to identify destabilizing KRAS mutations for the CPSEA study. A mutation library for $KRAS_{G12C}$ was constructed, and sotorasib was utilized to prioritize mutants exhibiting ligand-induced stabilization. Although the PSI distribution changes were moderately less pronounced than those observed in FKBP12 (Fig. 3c and 4a), we were still able to identify a subset of $KRAS_{G12C}$ mutants with decreased protein stability that were significantly improved upon sotorasib treatments (Fig. 4b and Supporting Information Fig. S4a). This is exemplified by the D119G/F156I double mutant, which exhibited the largest ligand-induced fluorescence differences (Fig. 4c). We thus designated $KRAS_{G12C}$ with this double mutation as DD-$KRAS_{G12C}$ (Fig. S4b).

In DD-$KRAS_{G12C}$-expressing cells, a variety of KRAS-targeting ligands, including adagrasib (a specific $KRAS_{G12C}$ inhibitor), BI2865 (a pan-KRAS inhibitor)[30], and MRTX1133 (a specific $KRAS_{G12D}$ inhibitor)[31], stabilized the DD-$KRAS_{G12C}$ protein alongside sotorasib at relatively high concentrations, leading to enhanced fluorescence signals and increased protein levels (Fig. S4c and d). To determine whether the destabilizing mutation, when introduced into wild-type KRAS and other KRAS G12 variants, can confer robust yet specific responses to KRAS inhibitors with distinct isoform selectivity, we generated DD-KRAS, DD-$KRAS_{G12C}$, DD-$KRAS_{G12D}$, DD-$KRAS_{G12V}$, and DD-$KRAS_{G12S}$ cell models (Fig. S4e). The ectopically expressed DD-$KRAS_{G12C}$ exhibited high specificity to the $KRAS_{G12C}$-selective ligands sotorasib and adagrasib (Fig. 4d and e, Fig. S4f), while DD-$KRAS_{G12D}$ was almost exclusively stabilized by MRTX1133 (Fig. 4f). Nevertheless, MRTX1133 demonstrated weak stabilization for other G12 mutants and wild-type KRAS, especially at higher doses (Fig. 4f). As expected, the pan-KRAS ligand BI2865 stabilized all DD-$KRAS_{G12X}$ variants (Fig. 4g and Fig. S4f). These results accentuate that our DD-$KRAS_{G12X}$

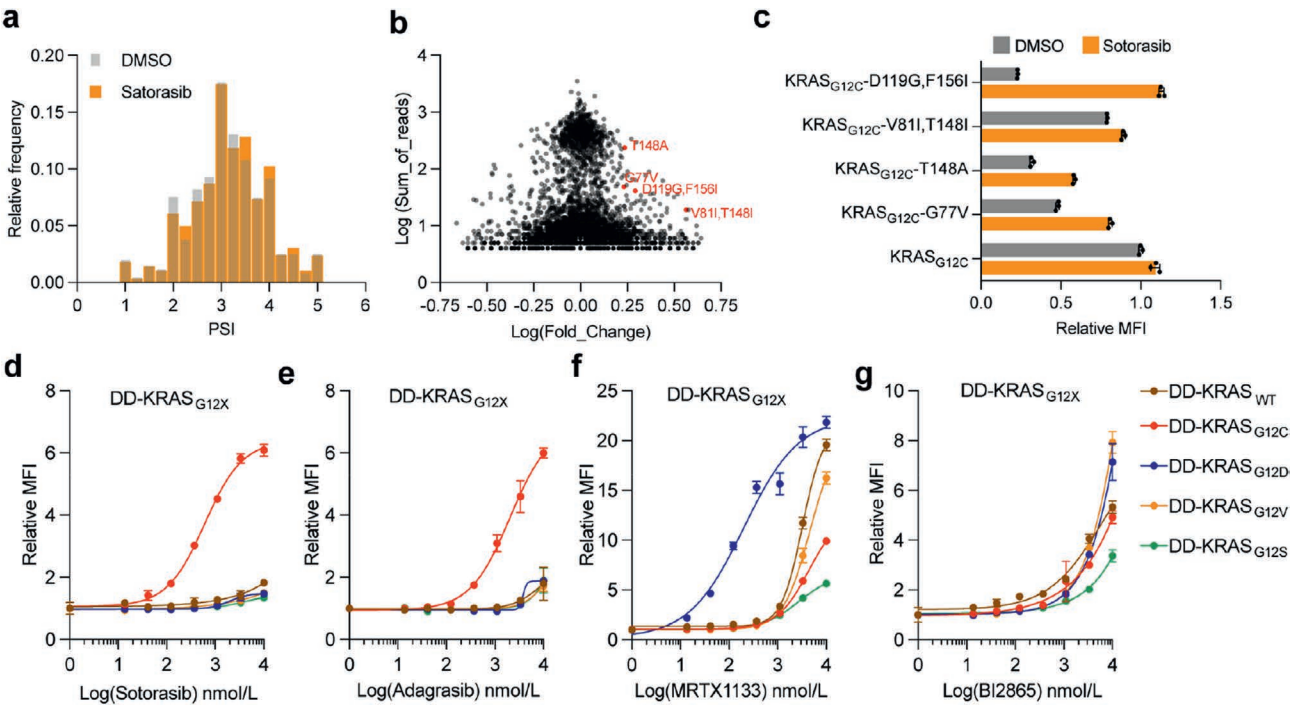

Figure 4 Identification and characterization of DD-KRAS. (a) Overall distribution of stability scores of mutant $KRAS_{G12C}$, comparing without ligand (grey) and sotorasib-treated (yellow) cells. (b) The distribution of sequencing reads and the stability changes of approximately 4700 mutant $KRAS_{G12C}$ before and after sotorasib treatment. The fold change represents the ratio of PSI in mutant cells after sotorasib treatment compared to untreated cells, while the sum of reads represents the total number of nucleic acid sequence reads from deep sequencing corresponding to each amino acid mutation. The red points were selected for subsequent experimental validation. (c) Histogram showing the relative MFI of various mutant $KRAS_{G12C}$. NIH3T3 cells expressing specified mutant $KRAS_{G12C}$ were treated with 5 μmol/L sotorasib or DMSO for 24 h, and MFI of EYFP was analyzed using flow cytometry. The relative MFI represents the MFI of cells relative to the MFI of DMSO-treated NIH3T3 cells expressing $KRAS_{G12C}$. (d–g) Dose-dependent stabilization of DD-$KRAS_{G12X}$-EYFP by sotorasib (d), adagrasib (e), MRTX1133 (f) and BI2865 (g). NIH3T3 cells expressing DD-$KRAS_{G12X}$-EYFP were treated with 13.7–10,000 nmol/L specified ligand for 24 h. Relative MFI represents the MFI of ligand-treated cells relative to the MFI of DMSO-treated cells. The data in (c–g) represent the mean ± SD from three technical replicates and the experiments were repeated three times.

cell model largely recapitulates the selectivity profiles of ligands targeting distinct KRAS mutants.

3.5. CPSEA identified colchicine as a KRAS binder with higher selectivity towards $KRAS_{G12S}$

To discover cellularly active ligands that interfere with oncogenic KRAS signaling, we implement a DD-$KRAS_{G12C}$-based HTS screening with an averaged Z' factor of 0.72 (Supporting Information Fig. S5a) using the L6000 compound library. This library consists of approximately 2500 natural products derived from over 2000 medicinal plants, animals, and microorganisms, encompassing more than 500 distinct molecular scaffolds. Compounds exhibiting a Z-score >3 (Fig. S5b) in the initial screening were triaged to exclude potential nuisances, such as compounds only active at extremely high concentrations or non-specifically enhancing fluorescence in the DD-CypA-EYFP model (Fig. S5c–e). This led to the identification of five trimethoxyphenyl-ring-containing compounds that stabilized DD-$KRAS_{G12C}$, with colchicine emerged as the most potent hit, exhibiting an EC_{50} value of 59 nmol/L (Fig. 5a–c). Erianin, a compound reported to bind $KRAS_{G13D}$ (Fig. S5f)[32], displayed weak activities in improving $KRAS_{G12C}$-EYFP protein stability (Fig. 5c and Fig. S5g). We further confirmed that the increased $KRAS_{G12C}$-EYFP protein levels induced by colchicine and erianin were not due to inhibition of the proteasome pathway or KRAS ubiquitination (Fig. S5h–j), nor attributed to transcriptional induction of KRAS (Fig. S5k).

Interestingly, the DD-$KRAS_{G12X}$ profiling experiment revealed that colchicine induced a relatively stronger upregulation of fluorescence signals in cells expressing DD-$KRAS_{G12S}$ compared to other isoforms, including DD-$KRAS_{G12C}$, particularly at higher concentrations (Fig. S5l and m). This encouraged us to perform a series of functional assays to assess colchicine's specificity for $KRAS_{G12X}$ isoforms without the use of destabilizing mutations. Firstly, CETSA experiments showed a significantly increased thermo stability of endogenous $KRAS_{G12S}$ and $KRAS_{G12D}$, with a lesser extent for $KRAS_{G12C}$, in cells treated with high concentrations of colchicine (Fig. S5n). Next, MST-based binding assays confirmed a direct and more potent interaction between colchicine and $KRAS_{G12S}$ compared to $KRAS_{G12C}$ and $KRAS_{G12D}$ (Fig. 5d). Molecular docking studies revealed that colchicine occupied the switch-II pocket of $KRAS_{G12S}$, partially overlapping with the binding region of known $KRAS_{G12S}$-selective inhibitor[19]. This binding is stabilized by extensive intermolecular contacts, including hydrogen bonds (H-bonds) between colchicine and the side chain of residue Y64 and the main chain of S12, as well as hydrophobic interactions with residues Y96, Y64 and E62 (Fig.

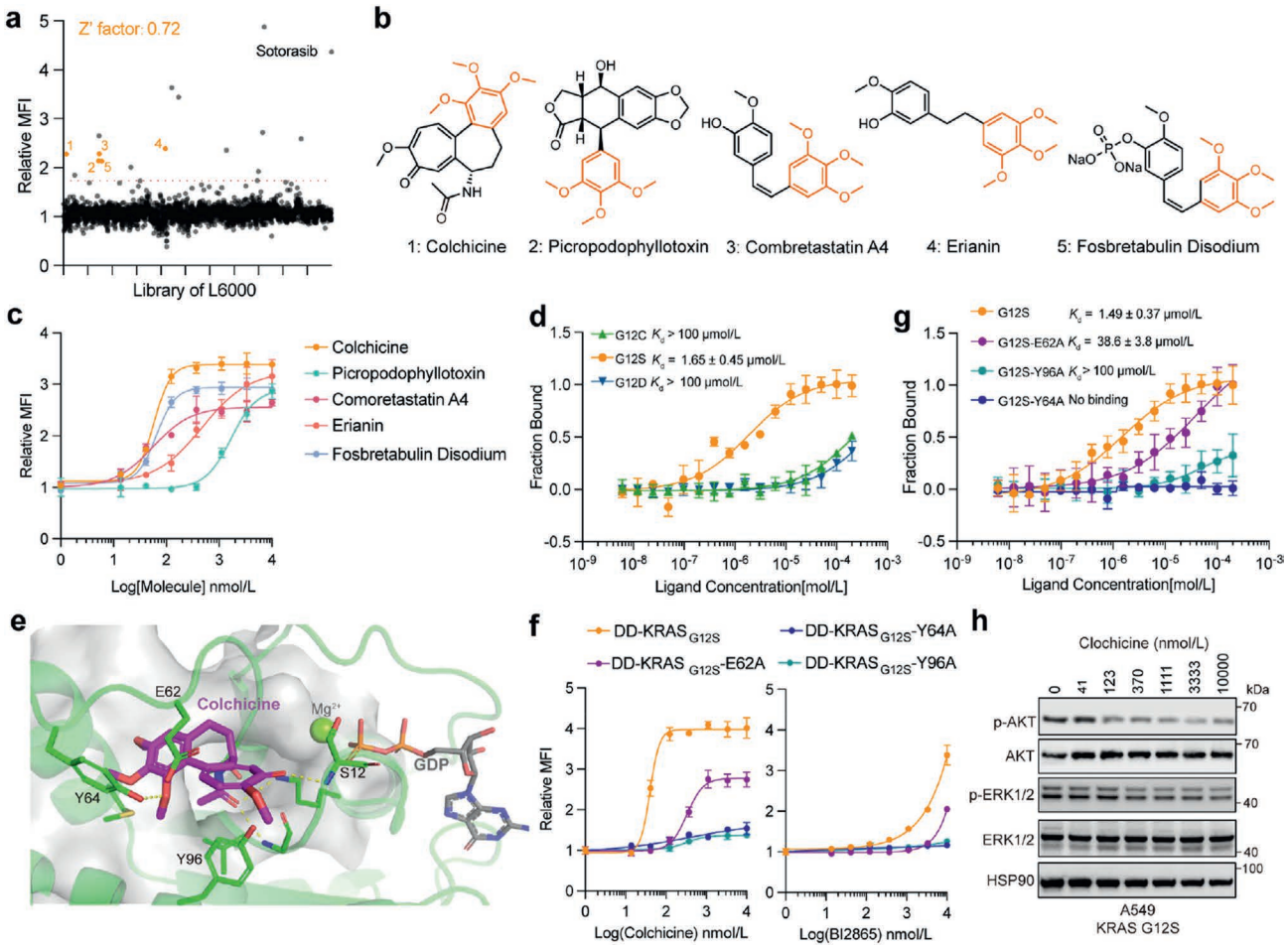

Figure 5 CPSEA identified colchicine as a KRAS binder with higher selectivity towards $KRAS_{G12S}$. (a) Scatter plot of primary screening data showing compounds from a library of L6000 that stabilize DD-$KRAS_{G12C}$. NIH3T3 cells expressing DD-$KRAS_{G12C}$-EYFP were treated with 5 μmol/L compounds for 24 h and the MFI of EYFP was analyzed using flow cytometry. Relative MFI represents the MFI of compound-treated cells relative to the MFI of DMSO-treated cells. The compounds labeled 1−5 are described in (b). (b) Structures of five compounds containing a trimethoxyphenyl ring (highlighted in orange) obtained through primary screening. (c) Dose-dependent stabilization of DD-$KRAS_{G12C}$-EYFP by various compounds. NIH3T3 cells expressing DD-$KRAS_{G12C}$-EYFP were treated with 13.7−10,000 nmol/L specified ligand for 24 h. Relative MFI represents the MFI of compound-treated cells relative to the MFI of DMSO-treated cells. Before analyzing the EYFP fluorescence signal, dead cell populations were excluded using PI dye. (d) MST assay showing the interaction between colchicine and KRAS variants. (e) Docking model of the colchicine and $KRAS_{G12S}$. The intermolecular H-bond contracts are indicated by yellow dashed-lines. (f) Dose-dependent stabilization of DD-$KRAS_{G12S}$-EYFP with different amino acid mutations by colchicine and BI2865. (g) MST assay showing the interaction between colchicine and $KRAS_{G12S}$ variants. (h) A549 cells were treated with colchicine for 24 h, and the effect on AKT and ERK1/2 signaling activation was measured by Western blot and the experiments were repeated twice. The data in (c, d, g, f) represent the mean ± SD from three technical replicates and the experiments were repeated twice.

5e). Consistently, colchicine-mediated DD-$KRAS_{G12S}$ stabilization was severely attenuated upon introducing the E62A, -Y64A, and -Y96A mutations (Fig. 5f), which also markedly reduced the binding affinities of colchicine to recombinant $KRAS_{G12S}$ proteins in MST assays (Fig. 5g), supporting the reliability of the docking model. The binding of colchicine with $KRAS_{G12S}$ led to effective inhibition of activated RAS (Fig. S5o) and its downstream signaling pathway in $KRAS_{G12S}$-expressing A549 cells (Fig. 5h). In contrast, RAS pathways showed no significant alterations in cells expressing wild-type or other KRAS variants (Fig. S5p). Collectively, these data suggest that incorporating destabilizing mutations substantially sensitized the detection of binding between $KRAS_{G12C}$ and colchicine, enabling the subsequent functional validation of colchicine's specific binding and inhibitory effects on $KRAS_{G12S}$.

3.6. Identification of destabilizing mutations in a ligand-independent manner

Given that many proteins lack appropriate ligands with sufficient affinity and specificity to identify destabilizing mutations for CPSEA studies, a more universal, ligand-independent strategy is necessary. Protein stability alterations are commonly quantified by the change in Gibbs free energy ($\Delta\Delta G$), and numerous computational approaches have been developed to estimate the $\Delta\Delta G$ values of mutant proteins[33]. Here, we employed the DDMut

model[34], which predicts mutation-induced protein stability changes using deep learning techniques, to compute $\Delta\Delta G$ values for FKBP12 mutants. Leveraging deep sequencing data from the mutant library, we defined a metric called folding fitness, which reflects the relative stability of a mutated protein compared to wild-type, calculated as the base-10 logarithm of the ratio between the PSI of the mutant and that of WT protein. The predicted $\Delta\Delta G$ values exhibited a significant positive correlation with experimentally measured folding fitness (Fig. 6a), suggesting that $\Delta\Delta G$ can serve as a reliable metric for assessing stability changes of mutant proteins.

By comparing the $\Delta\Delta G$ values of all possible FKBP12 single-point mutations with those of experimentally validated unstable mutations (Fig. 6b)[16], we found that although these destabilizing variants are distributed across the protein, most of them have $\Delta\Delta G$ values ranging from −2.5 to −1 kcal/mol, suggesting their

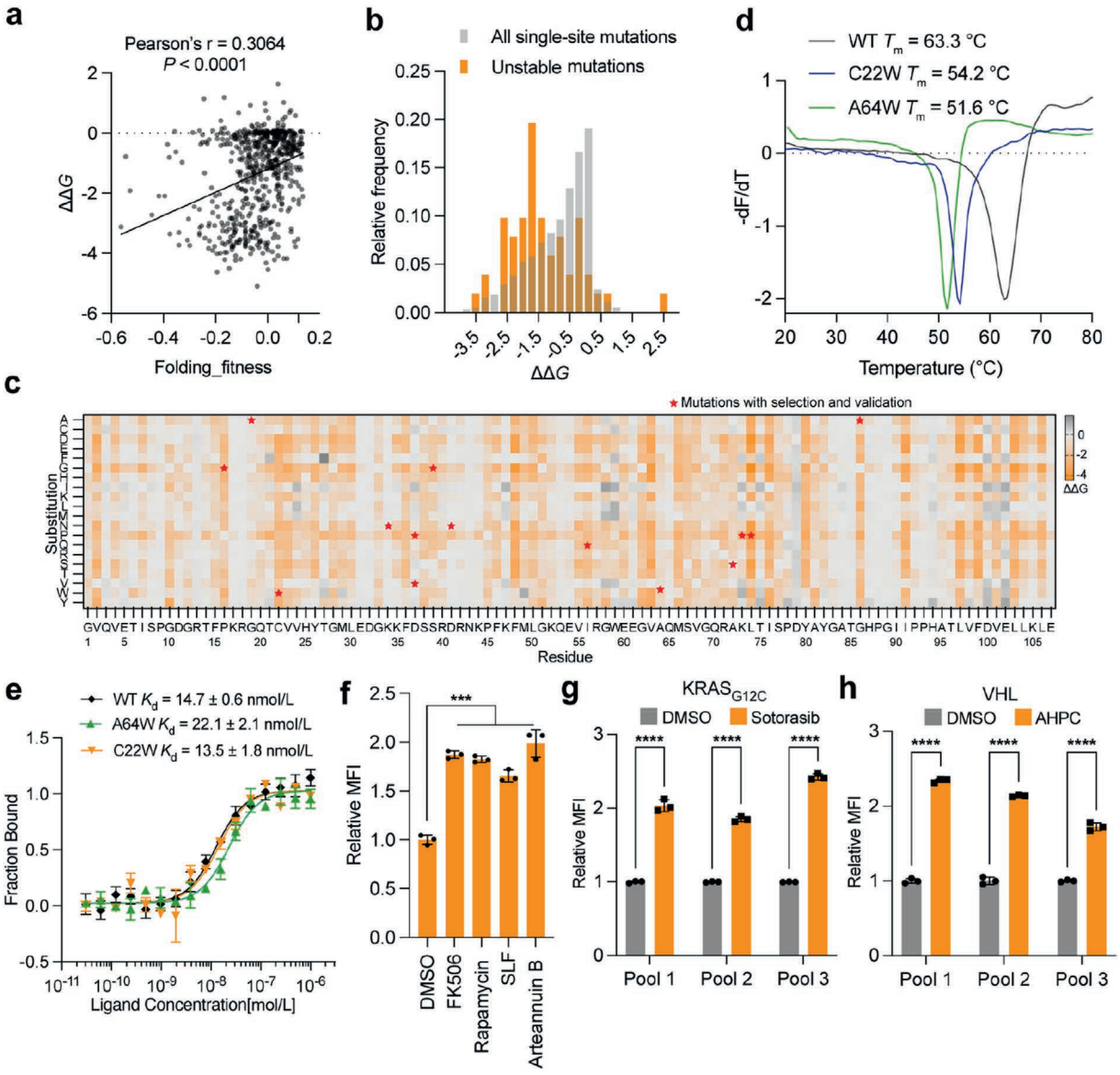

Figure 6 Identification of destabilizing mutations in a ligand-independent manner. (a) Scatter plot comparing folding fitness and $\Delta\Delta G$ of amino acid mutations in FKBP12. Pearson's r and P-value are shown. (b) Overall distribution of $\Delta\Delta G$ for mutant FKBP12, comparing all single-site mutations (grey) and unstable mutations (yellow). (c) Heatmap representation of the $\Delta\Delta G$ for the single-site mutant of FKBP12. The asterisk indicates the mutations selected for experimental validation. (d) TSA measuring the T_m of WT, C22W, and A64W FKBP12 proteins. Both mutants showed a significant decrease in T_m compared to WT, confirming their reduced stability. (e) MST analysis of FK506 binding affinity to mutant FKBP12. The C22W and A64W mutations had only a minor effect on binding affinity. (f) Histogram showing the relative MFI of cell pool with unstable FKBP12 obtained through $\Delta\Delta G$ treated by 5 μmol/L FK506, rapamycin, SLF and arteannuin B for 24 h. Relative MFI represents the MFI of compound-treated cells relative to the MFI of DMSO-treated cells. (g) Histogram showing the relative MFI of cell pools with unstable $KRAS_{G12C}$ obtained through $\Delta\Delta G$ treated by DMSO and 5 μmol/L sotorasib for 24 h. (h) Histogram showing the relative MFI of cell pools with unstable VHL obtained through $\Delta\Delta G$ treated by DMSO and 5 μmol/L (*S*,*R*,*S*)-AHPC-propargyl for 24 h. The data in (e−h) represent the mean ± SD from three technical replicates and the experiments were repeated twice. ***$P < 0.001$, ****$P < 0.0001$.

negative impacts on protein stability, a pattern similarly observed in CypA (Supporting Information Fig. S6a). Based on this, we selected a variety of previously uncharacterized mutants (Fig. 6c) that were also predicted to be destabilizing by GeoStab[35] and Duet[36] analyses (Fig. S6b), for experimental validation. Most mutants within the $\Delta\Delta G$ range from -2.5 to -1 kcal/mol showed markedly reduced stabilities that were readily rescued by FK506 treatment, whereas mutants outside this range exhibited only subtle-to-moderate ligand responses (Fig. S6c). We further confirmed that the C22W and A64W mutations significantly destabilized FKBP12 (Fig. 6d), which aligned with the $\Delta\Delta G$ predictions, while retaining FK506 binding capabilities comparable to those of the wild-type protein, akin to the effects observed for DD-FKBP12 (Fig. 6e). Notably, pooling cells expressing multiple predicted destabilizing FKBP12 mutants within this range could impart a robust signal window for CPSEA assay development (Fig. 6f).

The feasibility of this strategy was further demonstrated for $KRAS_{G12C}$ and the E3 ligase VHL. A global virtual mutagenesis scan was conducted using DDMut (Fig. S6d and f), followed by validation with GeoStab and Duet models. Single-site mutants exhibiting $\Delta\Delta G$ values between -2.5 and -1 kcal/mol were selected for plasmid construction, with 15 variants randomly divided into three groups (5 variants per group) (Fig. S6e and g). These plasmid pools were transduced into NIH3T3 cells to generate destabilized mutant cell pools. Upon ligand treatment, all cell pools demonstrated robust fluorescence enhancement (Fig. 6g and h). These results highlight that $\Delta\Delta G$ calculations represent a viable ligand-independent strategy to identify unstable mutations for POIs.

4. Discussion

To accelerate target-based drug discovery, we developed a cellular high-throughput ligand discovery method called CPSEA, which offers several key advantages. First, CPSEA enables the rapid identification of membrane-permeable compounds capable of binding to target proteins within the native cellular environment. This is particularly valuable for targets requiring post-translational modifications which are difficult to replicate *in vitro,* exemplified by p53, which depends on phosphorylation or acetylation[37]. Second, as a homogeneous assay, CPSEA eliminates the need for high-quality, target-specific antibodies and circumvents complex heating and centrifugation steps typical of CETSA, while maintaining high sensitivity for evaluating ligand−target engagement. This makes CPSEA a valuable, complementary approach to existing methods, such as the state-of-the-art HT-CETSA. Third, CPSEA enables identification of compounds that bind without necessarily inhibiting the target, providing valuable starting points for PROTAC development and targeted protein degradation. Fourth, our approach integrates both a deep sequencing-based experimental platform and a $\Delta\Delta G$-based computational approach to identify destabilizing mutations, thereby broadening CPSEA's applicability of across diverse POIs.

Interestingly, we found that coupling amplicon deep sequencing with FACS analysis outperformed traditional multi-round FACS selection[16] in identifying destabilizing KRAS mutations. This may be due to the metabolic burden imposed by continuous overexpression and degradation of destabilizing proteins, leading to growth disadvantages and loss of these cells during repeated selection rounds. Using this new approach, we obtained, to the best of our knowledge, the first destabilizing mutations for $KRAS_{G12C}$ and developed the DD-$KRAS_{G12X}$ profiling model, enabling the identification of colchicine as a $KRAS_{G12S}$-specific inhibitor with promising on-target effects in cells. Colchicine, a drug already used in the clinic known for gout[38], cardiovascular diseases[39], and cancer[40], could potentially be repurposed as a lead compound targeting KRAS mutation. Further studies are needed to elucidate its mechanisms in $KRAS_{G12S}$ inhibition. Moreover, we demonstrated the broad utility of the ligand-independent, computational prediction method for obtaining destabilizing mutations. Although not all predicted mutations exhibited robust ligand-stabilization responses, pooling multiple predicted mutations created cell pools with strong signal windows suitable for CPSEA assay development. Advances in artificial intelligence and structural prediction tools like AlphaFold will be instrumental in developing more accurate computational methods for predicting destabilizing mutations in POIs, further advancing CPSEA's capabilities. Additionally, replacing the EYFP reporter with alternatives such as NanoLuc[41], Hibit[42], or β-galactosidase[43] could expand the assay's readout options.

Although CPSEA provides a robust and comprehensive framework, highly complementary to other cellular high-throughput ligand discovery methods, several limitations remain. First, exogenously expressed POI-EYFP fusion protein may differ from that of the endogenous protein in terms of expression level, structure, localization, and ligand accessibility, which could influence target-small molecule interactions. This issue can be partially addressed by knocking in a smaller tag, such as Hibit, into the genomic POI loci. Second, destabilizing mutations might influence ligand-protein interactions by inducing conformational changes, potentially resulting in binding behavior that differs from that observed with the wild-type protein. These limitations, along with other factors like ligand permeability and serum binding, may collectively account for disparities between the half-maximal stability concentration derived from CPSEA and the *in vitro* binding affinity. Therefore, rigorous hit validation is essential to confirm direct ligand binding to recombinant wild-type proteins and target engagement *via* orthogonal assays like CETSA, while also ruling out transcriptional modulation of the POI and global perturbation of the ubiquitin−proteasome system. Notably, cases where intracellular target engagement cannot be recapitulated *in vitro* may reflect prodrug activation, conformational or functional differences between cellular and purified proteins, or context-specific microenvironmental effects. Further investigation is warranted to elucidate these mechanisms. Third, while we identified arteannuin B and colchicine as new, genuine binders for FKBP12 and $KRAS_{G12S}$, respectively, structural studies such as crystallography or cryo-electron microscopy (cryo-EM) will be necessary to elucidate their binding modes. These structural insights will be valuable for further optimizing the ligands into therapeutic agents with improved selectivity and potency.

In summary, CPSEA not only complements existing target-based approaches but also offers novel opportunities for high-throughput ligand screening in living cells, holding great promise for drug discovery.

Acknowledgments

This work was supported by grants from National Key R&D Program of China, Ministry of Science and Technology

(2024YFC2815900), National Natural Science Foundation of China (22277010, 92353303, 32200075 and 22477013), the R&D Program of Guangzhou Laboratory (GZNL2023A02003, China), the Major Research Project of GIBH (GIBHMRP2025-02, China), Natural Science Foundation of Chongqing (CSTB2025NSCQ-LZX0129, CSTB2022NSCQ-MSX1061, China), CQMU Program for Youth Innovation in Future Medicine (W0074, China), "Open bidding for selecting the best candidates" Project of the College of Pharmacy, Chongqing Medical University (YXY2024JBGS02, China), and the Strategic Priority Research Program of the Chinese Academy of Sciences (XDB1250000, China).

Author contributions

Yue Wei, Yongjun Dang, Xiangqian Kong and Zufeng Guo conceived the study and oversaw the project. Yue Wei and Yunyun Gao designed and conducted the main experiments. Wenjing Bai and Peirui Zhao were primarily responsible for FKBP12 protein purification, while Yao Chen and Ruijie Li carried out the MST experiments. Junchi Hu assisted with the $\Delta\Delta G$ calculations, and Linfeng Li performed molecular docking experiments. Xing Wang, Guobing Yin, Xiangqian Kong and Yongjun Dang provided valuable suggestions on the cell-related experiments. Yue Wei, Xiangqian Kong and Zufeng Guo drafted the manuscript, and all authors contributed to the discussion of results and provided feedback on the manuscript.

Conflicts of interest

The authors declare that they have no competing financial interests.

Data availability statement

The data that support the findings of this study are available from the corresponding author upon reasonable request.

Appendix A. Supporting information

Supporting information to this article can be found online at https://doi.org/10.1016/j.apsb.2026.02.008.

References

1. Crunkhorn S. Inhibiting protein−protein interactions. *Nat Rev Drug Discov* 2016;**15**:234.
2. Lin L, Yee SW, Kim RB, Giacomini KM. SLC transporters as therapeutic targets: emerging opportunities. *Nat Rev Drug Discov* 2015;**14**: 543−60.
3. Rask-Andersen M, Almen MS, Schioth HB. Trends in the exploitation of novel drug targets. *Nat Rev Drug Discov* 2011;**10**:579−90.
4. Sadri A. Is Target-based drug discovery efficient? Discovery and "off-target" mechanisms of all drugs. *J Med Chem* 2023;**66**:12651−77.
5. Brennan RJ, Jenkinson S, Brown A, Delaunois A, Dumotier B, Pannirselvam M, et al. The state of the art in secondary pharmacology and its impact on the safety of new medicines. *Nat Rev Drug Discov* 2024;**23**:525−45.
6. Martinez Molina D, Jafari R, Ignatushchenko M, Seki T, Larsson EA, Dan C, et al. Monitoring drug target engagement in cells and tissues using the cellular thermal shift assay. *Science* 2013;**341**:84−7.
7. Savitski MM, Reinhard FB, Franken H, Werner T, Savitski MF, Eberhard D, et al. Tracking cancer drugs in living cells by thermal profiling of the proteome. *Science* 2014;**346**:1255784.
8. Park C, Marqusee S. Pulse proteolysis: a simple method for quantitative determination of protein stability and ligand binding. *Nat Methods* 2005;**2**:207−12.
9. Lomenick B, Hao R, Jonai N, Chin RM, Aghajan M, Warburton S, et al. Target identification using drug affinity responsive target stability (DARTS). *Proc Natl Acad Sci U S A* 2009;**106**:21984−9.
10. Strickland EC, Geer MA, Tran DT, Adhikari J, West GM, DeArmond PD, et al. Thermodynamic analysis of protein−ligand binding interactions in complex biological mixtures using the stability of proteins from rates of oxidation. *Nat Protoc* 2013;**8**:148−61.
11. Feng Y, De Franceschi G, Kahraman A, Soste M, Melnik A, Boersema PJ, et al. Global analysis of protein structural changes in complex proteomes. *Nat Biotechnol* 2014;**32**:1036−44.
12. Cho KF, Ma TP, Rose CM, Kirkpatrick DS, Yu K, Blake RA. Chaperone mediated detection of small molecule target binding in cells. *Nat Commun* 2020;**11**:465.
13. Jafari R, Almqvist H, Axelsson H, Ignatushchenko M, Lundback T, Nordlund P, et al. The cellular thermal shift assay for evaluating drug target interactions in cells. *Nat Protoc* 2014;**9**:2100−22.
14. Almqvist H, Axelsson H, Jafari R, Dan C, Mateus A, Haraldsson M, et al. CETSA screening identifies known and novel thymidylate synthase inhibitors and slow intracellular activation of 5-fluorouracil. *Nat Commun* 2016;**7**:11040.
15. Dart ML, Machleidt T, Jost E, Schwinn MK, Robers MB, Shi C, et al. Homogeneous assay for target engagement utilizing bioluminescent thermal shift. *ACS Med Chem Lett* 2018;**9**:546−51.
16. Banaszynski LA, Chen LC, Maynard-Smith LA, Ooi AG, Wandless TJ. A rapid, reversible, and tunable method to regulate protein function in living cells using synthetic small molecules. *Cell* 2006;**126**:995−1004.
17. Weber EW, Parker KR, Sotillo E, Lynn RC, Anbunathan H, Lattin J, et al. Transient rest restores functionality in exhausted CAR-T cells through epigenetic remodeling. *Science* 2021;**372**. eaba1786.
18. Nabet B, Roberts JM, Buckley DL, Paulk J, Dastjerdi S, Yang A, et al. The dTAG system for immediate and target-specific protein degradation. *Nat Chem Biol* 2018;**14**:431−41.
19. Zhang Z, Guiley KZ, Shokat KM. Chemical acylation of an acquired serine suppresses oncogenic signaling of K-Ras(G12S). *Nat Chem Biol* 2022;**18**:1177−83.
20. Clackson T, Yang W, Rozamus LW, Hatada M, Amara JF, Rollins CT, et al. Redesigning an FKBP-ligand interface to generate chemical dimerizers with novel specificity. *Proc Natl Acad Sci U S A* 1998;**95**: 10437−42.
21. Chu BW, Kovary KM, Guillaume J, Chen LC, Teruel MN, Wandless TJ. The E3 ubiquitin ligase UBE3C enhances proteasome processivity by ubiquitinating partially proteolyzed substrates. *J Biol Chem* 2013;**288**:34575−87.
22. Flanagan WM, Corthesy B, Bram RJ, Crabtree GR. Nuclear association of a T-cell transcription factor blocked by FK-506 and cyclosporin A. *Nature* 1991;**352**:803−7.
23. Schreiber SL. Chemistry and biology of the immunophilins and their immunosuppressive ligands. *Science* 1991;**251**:283−7.
24. May EM. *Lessons from cyclosporine A: structural determinants of conformation-switching and passive membrane penetration*. Harvard University; 2015. Doctoral Dissertation.
25. Fischer G, Wittmann-Liebold B, Lang K, Kiefhaber T, Schmid FX. Cyclophilin and peptidyl-prolyl *cis−trans* isomerase are probably identical proteins. *Nature* 1989;**337**:476−8.
26. Fehr T, Kallen J, Oberer L, Sanglier JJ, Schilling W. Sanglifehrins A, B, C and D, novel cyclophilin-binding compounds isolated from *Streptomyces* sp. A92-308110. II. Structure elucidation, stereochemistry and physico-chemical properties. *J Antibiot (Tokyo)* 1999;**52**: 474−9.
27. Guo Z, Hong SY, Wang J, Rehan S, Liu W, Peng H, et al. Rapamycin-inspired macrocycles with new target specificity. *Nat Chem* 2019;**11**: 254−63.
28. Singhal A, Li BT, O'Reilly EM. Targeting KRAS in cancer. *Nat Med* 2024;**30**:969−83.

29. Yen HC, Xu Q, Chou DM, Zhao Z, Elledge SJ. Global protein stability profiling in mammalian cells. *Science* 2008;**322**:918−23.
30. Kim D, Herdeis L, Rudolph D, Zhao Y, Bottcher J, Vides A, et al. Pan-KRAS inhibitor disables oncogenic signalling and tumour growth. *Nature* 2023;**619**:160−6.
31. Hallin J, Bowcut V, Calinisan A, Briere DM, Hargis L, Engstrom LD, et al. Anti-tumor efficacy of a potent and selective non-covalent KRAS(G12D) inhibitor. *Nat Med* 2022;**28**:2171−82.
32. Miao Q, Deng WQ, Lyu WY, Sun ZT, Fan SR, Qi M, et al. Erianin inhibits the growth and metastasis through autophagy-dependent ferroptosis in KRAS(G13D) colorectal cancer. *Free Radic Biol Med* 2023;**204**:301−12.
33. Marabotti A, Del Prete E, Scafuri B, Facchiano A. Performance of web tools for predicting changes in protein stability caused by mutations. *BMC Bioinf* 2021;**22**:345.
34. Zhou Y, Pan Q, Pires DEV, Rodrigues CHM, Ascher DB. DDMut: predicting effects of mutations on protein stability using deep learning. *Nucleic Acids Res* 2023;**51**:W122−8.
35. Xu Y, Liu D, Gong H. Improving the prediction of protein stability changes upon mutations by geometric learning and a pre-training strategy. *Nat Comput Sci* 2024;**4**:840−50.
36. Pires DE, Ascher DB, Blundell TL. DUET: a server for predicting effects of mutations on protein stability using an integrated computational approach. *Nucleic Acids Res* 2014;**42**:W314−9.
37. Hafner A, Bulyk ML, Jambhekar A, Lahav G. The multiple mechanisms that regulate p53 activity and cell fate. *Nat Rev Mol Cell Biol* 2019;**20**:199−210.
38. Butt JH, Docherty KF, Claggett BL, Desai AS, Petersson M, Langkilde AM, et al. Association of dapagliflozin use with clinical outcomes and the introduction of uric acid-lowering therapy and colchicine in patients with heart failure with and without gout: a patient-level pooled meta-analysis of DAPA-HF and DELIVER. *JAMA Cardiol* 2023;**8**:386−93.
39. Deftereos SG, Beerkens FJ, Shah B, Giannopoulos G, Vrachatis DA, Giotaki SG, et al. Colchicine in cardiovascular disease: in-depth review. *Circulation* 2022;**145**:61−78.
40. Chen H, Deng S, Albadari N, Yun MK, Zhang S, Li Y, et al. Design, synthesis, and biological evaluation of stable colchicine-binding site tubulin inhibitors 6-Aryl-2-benzoyl-pyridines as potential anticancer agents. *J Med Chem* 2021;**64**:12049−74.
41. Hall MP, Unch J, Binkowski BF, Valley MP, Butler BL, Wood MG, et al. Engineered luciferase reporter from a deep sea shrimp utilizing a novel imidazopyrazinone substrate. *ACS Chem Biol* 2012;**7**:1848−57.
42. Dixon AS, Schwinn MK, Hall MP, Zimmerman K, Otto P, Lubben TH, et al. NanoLuc complementation reporter optimized for accurate measurement of protein interactions in cells. *ACS Chem Biol* 2016;**11**:400−8.
43. Husain Q. Beta galactosidases and their potential applications: a review. *Crit Rev Biotechnol* 2010;**30**:41−62.